

Toward generative machine learning for boosting ensembles of climate simulations

Parsa Gooya¹, Reinel Sospedra-Alfonso¹, and Johannes Exenberger^{2,3}

¹Canadian Centre for Climate Modeling and Analysis, Environment and Climate Change Canada, Victoria, British Columbia, Canada

²Vienna University of Technology

³Institute of Software Technology and Artificial Intelligence, Graz University of Technology

Key Points:

- A framework for conditional variational autoencoders is presented to generate large ensembles of climate data from limited training sample.
- Variational autoencoders learn the underlying distribution of data and generate ensembles with extremes beyond the limited training sample.
- Proper representation of output noise is key to avoid overly smooth outputs, spectral bias and loss of variability.

Abstract

Accurately quantifying uncertainty in predictions and projections arising from irreducible internal climate variability is critical for informed decision-making. Such uncertainty is typically assessed using ensembles produced with physics-based climate models. However, computational constraints impose a trade-off between generating the large ensembles required for robust uncertainty estimation and increasing model resolution to better capture fine-scale dynamics. Generative machine learning offers a promising pathway to alleviate these constraints. We develop a conditional Variational Autoencoder (cVAE) trained on a limited sample of climate simulations to generate arbitrary large ensembles. The approach is applied to output from monthly CMIP6 historical and future scenario experiments produced with the Canadian Centre for Climate Modelling and Analysis' (CCCma's) Earth system model CanESM5. We show that the cVAE model learns the underlying distribution of the data and generates physically consistent samples that reproduce realistic low- and high-moment statistics, including extremes. Compared with more sophisticated generative architectures, cVAEs offer a mathematically transparent, interpretable, and computationally efficient framework. Their simplicity lead to some limitations, such as overly smooth outputs, spectral bias, and underdispersion, that we discuss along with strategies to mitigate them. Specifically, we show that incorporating output noise improves the representation of climate-relevant multiscale variability, and we propose a simple method to achieve this. Finally, we show that cVAE-enhanced ensembles capture realistic global teleconnection patterns, even under climate conditions absent from the training data.

Plain Language Summary

We examine how generative machine learning methods can expand climate model ensembles used to quantify uncertainty arising from internal climate variability. Traditional ensemble approaches rely on computationally expensive physics-based climate models, creating a trade-off between ensemble size and model resolution. To address this, we train a conditional Variational Autoencoder (cVAE) on a limited set of monthly historical and scenario simulations from the Canadian Earth system model CanESM5. The cVAE learns the statistical structure of the training data and generates samples that preserve key physical characteristics, including realistic distributions, extremes, and large-scale spatial patterns. Although cVAEs exhibit limitations such as spectral bias and underdispersion, we analyze these behaviors and outline practical mitigation strategies. We demonstrate that adding output noise improves the representation of multiscale climate variability. The resulting cVAE-enhanced ensemble reproduces credible global climate relationships, even under climate conditions absent from the training data.

1 Introduction

The climate system is inherently chaotic, meaning that small perturbations of climate states amplify over time and make both seasonal-to-decadal (S2D) predictions and long-term projections fundamentally uncertain (Lai et al., 2025; Li et al., 2024). Quantifying this uncertainty is essential for risk assessment and informed decision-making in climate applications (Sacco et al., 2022). To represent uncertainty, climate modeling typically relies on simulation ensembles, with each member of the ensemble representing a possible realization of the climate system. For S2D predictions (spanning a few months to ten years), ensemble members are initialized with slightly perturbed initial states to sample a range of plausible climate trajectories driven by predictable modes of internal variability, such as El Niño-Southern Oscillation (ENSO), and by external forcing, such as greenhouse gasses and volcanic aerosols (Merryfield et al., 2020; Boer et al., 2013; Sospedra-Alfonso & Boer, 2020). For long-term projections (spanning several years to over a century), simulations are instead initialized from sufficiently different climate states to span

slow-evolving internal variability, with predictability arising only from the imposed external forcing. In this context, the spread across the ensemble provides an estimate of long-term uncertainty, and broader, more thoroughly sampled ensembles offer a more reliable representation of the range of realizable climate states under a given forcing (Gooya et al., 2023; Lehner et al., 2020; Leutbecher, 2019). Consequently, large ensembles are necessary for a robust estimation of the long-term uncertainty arising from both fast- and slow-evolving variability as well as to estimate the likelihood of low probability high impact extreme events. In practice, ensemble size is constrained by computational cost, imposing trade-offs between model resolution and the number of ensemble members that can be feasibly produced (Sospedra-Alfonso et al., 2021; Swart et al., 2019a).

Recent advances in deep learning and generative machine learning have enabled the weather prediction community to substantially reduce the cost of ensemble forecasting (Lai et al., 2025; Li et al., 2024). These efforts range from improving prediction system output statistics, such as the spread of deterministic prediction ensembles (Sacco et al., 2022) and probabilistic forecasts (Grönquist et al., 2021), to data-driven generation of high-dimensional weather-like samples from target forecast distributions (Li et al., 2024). Generative models extract statistical priors that support conditional or unconditional sampling of learned probability distributions (Li et al., 2024), increasing computational efficiency for tasks that traditionally required large computing resources with physics-based models. For climate modeling, applications include probabilistic regional downscaling (Lopez-Gomez et al., 2024; Daust & Monahan, 2024), simultaneous emulation and downscaling of climate models (Lupin-Jimenez et al., 2025), and probabilistic climate model emulation (Rühling Cachay et al., 2024; Barthel Sorensen et al., 2024; Sorensen et al., 2024; Wang et al., 2025), with generative ML emulators showing notable promise in the prediction of extreme event statistics by learning corrections to reduced complexity climate simulations such as outputs from a coarsely resolved numerical model (Sorensen et al., 2024) or an auto-regressive Gaussian emulator (Wang et al., 2025).

In this study, we employ a conditional Variational Autoencoder (cVAE) (Kingma & Welling, 2022; Rezende et al., 2014) to generate arbitrary large samples of monthly near-surface air temperature (TAS) under historical or future scenario forcing. We are interested in learning the monthly TAS distribution of events over multi-decade time-scales consistent with the underlying climate. cVAEs are generative models that learn low dimensional representations of data and generate new data samples while conditioning on relevant information to control the generation process. They consist of an encoder network that maps the input data to a probability distribution over a latent space, often a multivariate Gaussian, and a decoder network that reconstructs the original data from samples drawn from this latent distribution (Prince, 2023; Dorta et al., 2018). Here, we condition both the encoder and decoder on a low rank representation of the input data that capture the warming trend to constrain and guide the distribution of the model's output. This approach is suitable for climate ensemble generation tasks for which the data vary according to a potentially predictable component (i.e., externally forced and, in the case of predictions, internally generated due to, e.g., ENSO) and a component that is not predictable (i.e., weather-induced noise or, in the case of long-term projections, all internally generated variability). The expectation is that cVAEs learn representations of modes of variability conditioned on the dominant predictable components and generate unseen climate fields consistent with the learned modes. We chose cVAEs over more sophisticated generative models because of their straightforward and efficient training, their foundation in closed-form mathematical principles, and their greater interpretability. Our goal is not to design the most permanent model, but to show that inexpensive generative deep learning models trained on relatively small data samples can be used to produce ensembles of climate simulations with realistic behavior in both low- and high-order statistics, including the representation of extremes. Remarkably, we train our cVAE model on a *single* realization of CCCma's Earth system model CanESM5 (Swart et al., 2019a) and generate an arbitrary large ensemble of physically meaningful realizations.

The generated ensemble is evaluated against the full ensemble of CanESM5 simulations that does not include the member used for training. Since the data used for training spans a sufficiently long period relative to the frequency of events assessed (e.g., ENSO events generated from 40-year training data), training on one member is sufficient for cVAE’s performance. However, for a proper estimation of long-term uncertainty, training on more ensemble members and/or conditioning on the ensemble mean over two or more members is more appropriate. For predictions, on the other, a single member may suffice. We expand on this point in section 2.2.

The remainder of the paper is organized as follows. cVAEs are introduced in section 2.1. Data and data preprocessing are discussed in section 2.2. The cVAE model and the training process are given in section 2.3, while details of the model inference are presented in section 2.4, respectively. An important aspect of model inference is accounting for residual noise that is not learned during training. Section 2.5 examines the impact of including decoder noise during inference. Results and discussions are given in section 3. Section 4 ends with the conclusions.

2 Data and Methods

2.1 Generative model

Conditional variational autoencoders (cVAEs) (Kingma & Welling, 2022; Rezende et al., 2014; Sohn et al., 2015) are deep generative models that learn representations of high-dimensional distributions by formulating them as a “variational inference” problem. A cVAE defines a joint distribution between the input data space \mathcal{X} and an unobserved dimensionally-reduced latent space \mathcal{Z} (Szwarcman et al., 2024; Ghosh et al., 2020), conditioned to c . The latent variable z can be regarded as a lower-dimensional representation of x coming from the conditional prior distribution $p(z|c)$.

The generative process of cVAE consists of first generating a set of latent variables $z \in \mathcal{Z}$ from a prior distribution $p(z|c)$, and then generating (sampling) the data $x \in \mathcal{X}$ according to the output distribution function $p_\theta(x|z, c)$, usually parameterized as a Gaussian (Sohn et al., 2015). The distribution $p_\theta(x|z, c)$, known as the generative model or a probabilistic *decoder*, is derived using a neural network with parameters θ . These are estimated through the maximum likelihood of the generated samples (Sohn et al., 2015), a challenging task that involves the intractable posterior $p(z|x, c)$. Consequently, a distribution $q_\phi(z|x, c)$ known as the “recognition” model is introduced, often assumed to be a Gaussian, to approximate the true posterior $p(z|x, c)$ (Kingma & Welling, 2022; Sohn et al., 2015). The recognition model is derived using a separate neural network of parameters ϕ , known as the probabilistic *encoder*.

Following Kingma and Welling (2022), Sohn et al. (2015) showed that the parameters θ and ϕ for the cVAE can be efficiently estimated using the stochastic gradient variational Bayes (SGVB) framework, where the variational lower bound of the log-likelihood is used as a surrogate objective function:

$$\begin{aligned} \log p(x|c) &= KL(q_\phi(z|x, c) \| p(z|x, c)) + \mathbb{E}_{q_\phi(z|x, c)} [-\log q_\phi(z|x, c) + \log p(x, z|c)] \\ &\geq -KL(q_\phi(z|x, c) \| p(z|c)) + \mathbb{E}_{q_\phi(z|x, c)} [\log p_\theta(x|z, c)], \end{aligned} \quad (1)$$

In Eq. 1, the term KL is the Kullback–Leibler divergence and the second term is the expectation of the log-likelihood of samples over the distribution $q_\phi(z|x, c)$ (Prince, 2023). Together, both the *encoder* and *decoder* models form the conditional variational autoencoder. The full derivation of Eq. 1 is provided in the supplements.

To facilitate the computation of gradients with respect to the parameters of the encoder neural network, the reparameterization trick is used (Kingma & Welling, 2022). Assuming a standard Gaussian distribution for the latent variables, the first term of Eq. 1 has a closed form, while the second term can be approximated by drawing samples $z^{(l)}$ ($l = 1, \dots, L$) from the Gaussian approximation to the posterior distribution (recognition model) $q_\phi(z|x, c)$. This reduces the objective function to:

$$\mathcal{L}(x; \theta, \phi) = \frac{1}{2} \sum_{i=1}^k (1 + \log(\sigma_i^2(x, c)) - \mu_i^2(x, c) - \sigma_i^2(x, c)) + \frac{1}{L} \sum_{l=1}^L \log p_\theta(x|z^{(l)}, c), \quad (2)$$

which is to be maximized with respect to the parameters θ and ϕ . Here $\mu_i(x, c)$ and $\sigma_i(x, c)$ are the means and standard deviations of $q_\phi(z|x, c)$ for the latent dimensions $i = 1, \dots, k$. We emphasize that θ and ϕ denote the parameters of the neural networks used to determine the decoder and encoder distributions, respectively, and are not to be mistaken for the parameters of the distributions.

The cVAE model is thus formulated as follows:

$$\begin{aligned} \text{Encoder: } q_\phi(z|x, c) &= \mathcal{N}(\mu_{NN_\phi}(x, c), \sigma_{NN_\phi}^2(x, c)I) \\ \text{Decoder: } p_\theta(x|z, c) &= \mathcal{N}(\mu_{NN_\theta}(z, c), \sigma^2 I) \\ \text{Prior: } p(z|c) &= p(z) = \mathcal{N}(0, I) \end{aligned} \quad (3)$$

where I is the identity matrix and σ^2 is a location independent (constant) decoder noise. The encoder maps the input images $x \in \mathcal{X}$ into distributions over the latent space whose mean and standard deviation are output from the neural network and form $q_\phi(z|x, c)$, the Gaussian approximation to the posterior distribution. The decoder then maps the samples in the latent space back to the data space \mathcal{X} . Under this formulation, the second term in the cVAE loss function (Eq. 2) is proportional to the Mean Square Error (MSE) of the generated samples (see supplements), which encourages accurate reconstructions of data samples, and the KL divergence term regularizes a structured latent distribution. With this loss function, the cVAE learns the conditional distribution of the data through a lower dimensional latent representation that extracts information useful to generate data instances in a structured and continuous latent space. In the output space, the decoder models through $\mu_{NN_\theta}(z, c)$ the important aspects of the data as explained by the latent variable z , and the remaining unmodeled aspects are ascribed to the noise $\sigma^2 I$ (Prince, 2023). While the noise is usually assumed to be unstructured and independent of the data, we show that the decoder noise becomes especially important for climate data where multi-scale variability exists. In section 2.4, we describe our approach to approximate the decoder noise and how it can relate to model failures, underdispersivity, and loss of fine-scale variability.

2.2 Data and preprocessing

We employ monthly values of near-surface air temperature (TAS) spanning 75 years (1951-2025), produced with the Canadian Earth System Model version 5 (CanESM5) (Swart et al., 2019a) under CMIP6's historical and SSP2-4.5 scenario forcing (Eyring et al., 2016). The raw CanESM5 ensemble has 25 realizations of approximately 2.8° spatial resolution (64×128 in lat \times lon), generated from different initial conditions that are produced from 50-year intervals of a piControl simulation. This would capture a range of realizable internal variability of the model's climate. From the 25-member ensemble, we select a single ensemble member for training, grossly under-sampling CanESM5's climate and its extreme events. The goal is to boost the ensemble size of our extremely lim-

ited training sample to generate TAS fields with distributions consistent with CanESM5’s climate, including extremes.

For this task, we train a cVAE model to reconstruct monthly TAS maps conditional on a compressed low dimensional embedding of the same input fields. For training, we use data from the full period (1950-2020) and reserve (2021-2025) for validation (Sec. 2.3 and S2). We standardize the input by removing the monthly climatology and dividing by the monthly standard deviation across all training years, at each grid cell. As a result, the cVAE model focuses on learning the interannual variability of the data conditioned on the state of the climate extracted through condition embedding. The compressed condition embedding only learns the dominant mode of variability in the data. Therefore, it is expected to learn a signal close to the dominant predictable components that are common to the generated ensemble. When training on a single realization, as we do here, this is reminiscent of seasonal-to-decadal predictions, as the conditioning learns the forced component and a phased-locked realization of internally generated variability (e.g., ENSO). For climate projections, a conditioning that better isolates the forced component (e.g., average over several ensemble members, warming due to greenhouse gases) would be desirable. Given our time frame of analysis of the generated ensemble based on events that evolve on monthly to interannual time scales, training on a single ensemble member suffices.

2.3 Model and training

We use multilayer perceptrons (MLPs) for the encoder and decoder networks, with a latent variable $z \in \mathbb{R}^k$, $k = 500$, and a standard Gaussian prior that is *condition independent* (i.e. $p(z|c) = p(z) = \mathcal{N}(0, I)$). This is a reasonable assumption, as the goal is to learn the internal variability of the climate on interannual time scales. For condition embedding, we use a separate MLP denoted $F_{NN}(x)$ that outputs an embedding vector $c \in \mathbb{R}^2$ passed to both the encoder and the decoder. Details on network architectures are given in the supplements. Importantly, in such limited data regime (840 data points), the simplicity of the model is important since overly parametrized models are prone to overfitting.

The choice of a much lower dimension for the condition embedding compared to the latent space is necessary for two reasons. First, we want the condition embedding network to extract only the dominant predictable signals rather than focusing on residual variability specific to the realization used for training. For example, Fig. S1 shows that the condition embedding learns mainly the long-term trend. Second, since the condition embedding is extracted from the same TAS field that is being reconstructed, if the embedding contains enough information to skillfully reconstruct the input, then the KL penalty encourages the network to ignore the latent space and only rely on the condition to minimize KL in the loss function. This is a phenomenon known as “posterior collapse” (Sankarapandian & Kulis, 2021), which implies that the network essentially collapses to a deterministic autoencoder. Therefore, a bottle-neck conditioning vector is necessary.

Additionally, we employ beta annealing (Sankarapandian & Kulis, 2021) during training, a technique to linearly scale the weight of the KL divergence term in the loss function from 0 to 1 over the first 10 epochs during training. In this way, by slowly increasing the weight of the KL constraint in the latent space, the network starts as a simple autoencoder using the latent space together with the condition embedding for accurate reconstruction of TAS fields, which helps with learning a meaningful latent space. Posterior collapse where KL loss asymptotically approaches zero is then tracked from the training/validation KL divergence. We use batch size of 100 and a cosine decreasing learning rate with a starting maximum of 0.0001. The validation set is used to monitor pos-

terior collapse and apply early stopping if the validation MSE does not improve over 15 epochs. Training the cVAE takes less than 10 minutes on a single GPU.

2.4 Inference

Once trained, the model can be used to generate an arbitrarily large sample at each time instance using a conditioning field (i.e., a temperature map at a specific time), by sampling the latent space according to $p(z)$, decoding the samples with the conditional generative decoder, and sampling the decoder distribution (Eq. 3). This combined inference process takes a few seconds to run on a single GPU. We condition on TAS fields from a single ensemble member (same realization used for training) and generate 24-member ensembles to compare with the remainder 24 members out of the raw 25-member ensemble from CanESM5 (we refer to this ensemble as the population excluding train sample). We further apply a mean bias correction to the annual average of the generated TAS fields relative to the same conditioning input. The protocol for sample generation is described next.

The k -dimensional normal prior $\mathcal{N}(0, I)$ in cVAE models is often chosen to simplify the latent sampling $z^{(m)} \in \mathbb{R}^k$ ($m = 1, \dots, M$) at generation or inference time. During training, the KL term in the loss function serves as a regularization constraint to encourage learning a latent space where samples fall under this normal distribution. While one can adjust the weight of the KL term in the loss function (Eq. 1), i.e. $(1 + \beta) KL(q_\phi(z|x, c) \| p(z|c))$ with $\beta \geq 0$ (Sohn et al., 2015), latent samples do not always fall perfectly under the prior normal distribution (An & Jeon, 2023) where they could be more spread out in one dimension or have small covariance between dimensions. This is particularly important at inference time when generating extremes and producing samples that reflect the correct tail probabilities (Oliveira et al., 2022). To account for this, we could leverage the explicit formulation of the cVAE latent space and use the distribution of the encoded training data to guide inference sampling (Prince, 2023; Oliveira et al., 2022; Mooers et al., 2021; Hsieh & Wu, 2024). For instance, scaling the standard deviation of the prior distribution at inference time has been shown to provide an efficient control for synthesis towards more extreme scenarios and a wider range of internal variability (Oliveira et al., 2022; Gooya & Sospedra-Alfonso, 2025). Here, we approximate the Gaussian prior at inference time with the covariance matrix Σ_z^{train} whose structure is acquired from the latent encodings of the training samples via the posterior $q_\phi(z|x, c)$,

$$\Sigma_z^{train} = \overline{(Z - \bar{Z})(Z - \bar{Z})^\top} \quad (4)$$

where

$$Z = \begin{bmatrix} z_1^\top \\ z_2^\top \\ \vdots \\ z_N^\top \end{bmatrix}, \quad z_i \sim q_\phi(z | x_i, c_i) \quad (5)$$

for x_i, c_i pairs from the training dataset of size N . Therefore, at inference time we sample from the prior distribution $\mathcal{N}(0, \Sigma_z^{train})$.

Each latent sample generated with this prior distribution is mapped into the output space with the decoder, following a Gaussian distribution with mean $\mu_{NN_\theta}(z, c)$ and variance given by the decoder noise (Eq. 3). The variability in the decoder output is (implicitly) taken as minimal when the mean is used as the output, which is often the case

in regression based machine learning tasks. For TAS data however, one can expect high frequency unpredictable variability (e.g., resulting from weather noise) superimposed to the variability explainable by $\mu_{NN_\theta}(z, c)$ in the decoder, which the VAE model is likely to filter out through the bottle-neck latent variable. Therefore, representing such meaningful noise in the decoder on top of $\mu_{NN_\theta}(z)$ is important to avoid overly smooth fields. We note that the same could be true for any model trained with MSE as reconstruction loss, where the output converges to the mean of all possible learnable functions that vary depending on finite training data (Goodfellow et al., 2016). Now, modeling decoder variability with a constant diagonal matrix is based on the simplifying assumption that the noise is unstructured, random, and location-independent. While that might be the case for optimally-learned neural networks with sufficiently expressive architectures, this is not true in general. Dorta et al. (2018) argue that while the noise is commonly considered as unstructured inherent in the data, reconstruction errors (or residuals from the mean in the decoder Gaussian) are often caused by data deficiencies, limitations in the model capacity (e.g., suboptimal architecture) and suboptimal parameter estimation. Consequently, the decoder's variability is generally structured.

In principle, one can relax the unstructured noise assumption and learn location-dependent noise using a neural network. For example, Dorta et al. (2018) learn the noise structure using a multivariate Gaussian distribution with a sparse covariance matrix (*Decoder*: $\mathcal{N}(\mu_{NN_\theta}(z, c), \Sigma_{NN_\theta}(z, c))$) as a function of the data. We follow a simpler approach and estimate a covariance matrix from the residuals of the training data. Specifically, we estimate the covariance noise structure from the errors in the reconstruction of the training data. That is, we use the decoder distribution $\mathcal{N}(\mu_{NN_\theta}(z, c), \Sigma_x^{train})$ with

$$\Sigma_x^{train} = \overline{(X_{res} - \overline{X_{res}})(X_{res} - \overline{X_{res}})^T} \quad (6)$$

where

$$X_{res} = \begin{bmatrix} x_1 - \mu_{NN_\theta}(z_1, c_1)^T \\ x_2 - \mu_{NN_\theta}(z_2, c_2)^T \\ \vdots \\ x_N - \mu_{NN_\theta}(z_N, c_N)^T \end{bmatrix}, \quad z_i \sim q_\phi(z | x_i, c_i) \quad (7)$$

We therefore update the cVAE in Eq. 3 and proceed with the following model at inference time,

$$\begin{aligned} \text{Decoder: } & p_\theta(x|z, c) = \mathcal{N}(\mu_{NN_\theta}(z, c), \Sigma_x^{train}) \\ \text{Prior: } & p(z|c) = p(z) = \mathcal{N}(0, \Sigma_z^{train}) \\ \text{Condition: } & c = F_{NN}(x) \end{aligned} \quad (8)$$

where Σ_z^{train} and Σ_x^{train} are given by Eqs. 4 and 6, respectively, and F_{NN} is the MLP model mapping the input space to \mathbb{R}^2 .

2.5 Evaluation of cVAE with and without decoder noise

To assess the impact of decoder noise, Fig. 1a shows quantile-quantile (QQ) plots for the model output with decoder noise (VAE+DN) and without decoder noise (VAE) relative to the raw ensemble (population). The QQ plots are produced by pooling anomalies for all months and grid cells (i.e., after removing the seasonal cycle), with anomalies computed from monthly climatology over 1980-2020. We include the QQ plot for the anomalies in the training data for comparison. For a more complete assessment of variability,

Figs. 1b,c show the radially averaged power density (RAPSD) for the winter (DJF) and summer (JJA) seasons, while Figs. 1d-f show standard deviation maps. The maps show standard deviation at each location based on the pooled anomalies, while RAPSD is computed for each seasonal mean anomaly map by radially averaging its 2D Fourier spectra around the origin of the frequency domain (Nerini et al., 2017).

For VAE, the model underestimates the variability of the population, as indicated by the relatively shallow slope of the QQ curve (Fig. 1a). This muted variability is most pronounced on land and in the extratropical oceans (Figs. 1d,e), but it is also underestimated in the tropical Pacific, implying a relatively weak representation of ENSO in the VAE ensemble. In contrast, the addition of decoder noise in VAE+DN helps counteract this reduced variability, leading to clear improvements globally (Figs. 1d,e,f) and across both the lower and upper percentiles of the anomaly distribution (Fig. 1a). The power spectra curves show (Fig. 1b,c) an overall improvement in spatial variability for VAE+DN compared to VAE (which is mostly biased low) or the training sample, most notably during winter, indicating the benefits of decoder noise. However, for finer spatial scales (below ~ 200 kms), VAE+DN overestimates the population variability. While the coarse 64×128 grid size of TAS fields makes the estimation of power over fine resolution noisy, the error could also reflect the coarse resolution of CanESM5 and the limited ability of the raw ensemble to capture true fine-scale variation (section 2.2). Overall, our results show that the addition of decoder noise consistently enhances model performance, and therefore we adopt the VAE+DN configuration as our default going forward, unless otherwise noted. We expect more expressive architectures and higher spatial resolution in the data to improve the biases in the original VAE decoder. However, the VAE decoder can be improved insofar as the predictability limit of the system has not been reached (Subich et al., 2025).

3 Results and discussions

3.1 Regional statistics

The main purpose of boosting climate simulation ensembles is to accurately assess statistical properties of climate events, including extremes, which is not possible using a single realization or small ensembles. This is especially important for populated regions, where extreme events can lead to widespread disruptions. As an initial evaluation, we compare the VAE+DN boosted ensemble with the full CanESM5 ensemble (population) over the 1980-2020 period for model grid cells covering Vancouver, London, Hong Kong and Los Angeles, through QQ plots and probability density functions (PDFs) of anomalies from monthly climatology (Fig. 2).

The QQ plots (Fig. 2a,c,e,g) show that the VAE+DN model reproduces the percentiles of the anomaly distribution in the population, generally improving over the training sample for both the lower and upper percentiles. One exception is Vancouver, where the VAE+DN model overestimates the upper percentiles for reasons we examine below. To assess the model's ability to capture the distribution tails and extremes in the population, Fig. 2b,d,f,g shows the log PDFs for all locations. Overall, the boosted ensemble successfully captures events in the population that are absent from the training data, indicating the VAE+DN model's ability to generalize for out-of-training data. In the case of Vancouver, the model clearly represents events in the distribution tail that are not present in the population. This may be in part due to (1) limited training data being non-representative of possible asymmetric behavior (as seen in Fig. 2d) (2) the decoder tendency to produce symmetric distributions or (3) because the model generates relatively strong warming possibly tied to a learned relationship in the data. As we will see in the next section, Vancouver is within the ENSO teleconnection region known for El Niño-induced warming. Regarding (2), we note that the boosted ensemble is nevertheless able to capture

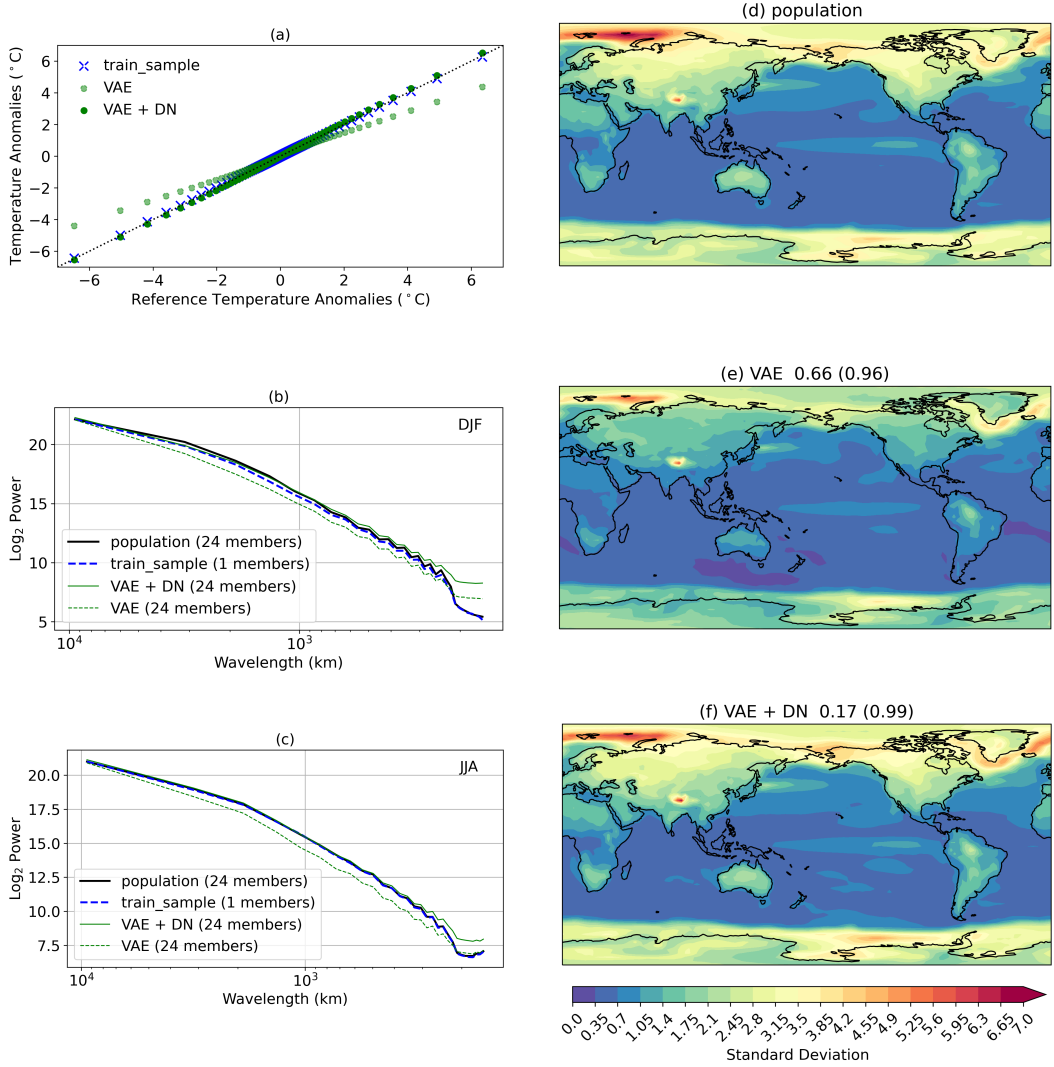


Figure 1: a) QQ plots of TAS anomalies relative to the seasonal climatology pooling all grid cells and times. b, c) Spectral power for DJF and JJA mean TAS anomalies averaged over years and realizations. d, e, f) standard deviation of TAS fields per grid cell across all times and realizations for different datasets. The numbers in the title of the panels are RMSE (pattern correlation) relative to the population on panel (d). All panels cover 1980-2020 period.

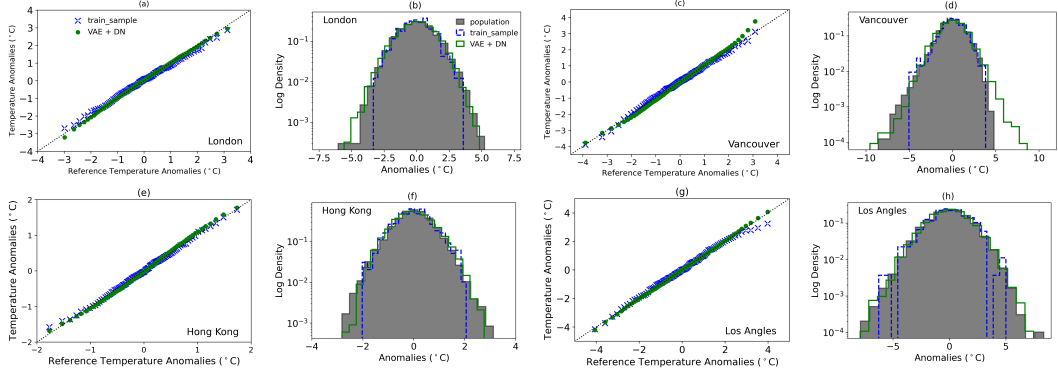


Figure 2: a, c, e, g) QQ plots of TAS anomalies relative to the seasonal climatology at different cities. b, d, f, h) PDF histograms on log scale for the same cities.

non-Gaussian behavior at these locations as shown with some detail in the supplements (Fig. S2).

To further assess the ability of the boosted ensemble to represent the TAS distribution in the population, particularly potential asymmetries and non-Gaussian behavior, Figs. 3a-d show measures of the third and fourth moments of the TAS distribution in the form of skewness and excess kurtosis. Figures 3a,c show that the population is characterized by higher latitudes with non-symmetric distributions and heavy tails, coincident with regions of strong variability (Fig. 1d). The VAE+DN boosted ensemble captures these global patterns but with underestimated magnitudes (Figs. 3b,d). This underestimation is not uncommon, even for more expressive architectures and larger training samples (Wang et al., 2025), although our limited training data may play a role. We examine whether our approach to estimate the noise in the decoder as a Gaussian with a constant covariance matrix independent of the generated output (Eq. 8), impacts skewness and kurtosis (Fig. S3 of the supplements). The results confirm that the asymmetric behavior of the distribution is better represented without decoder noise, while kurtosis (tail behavior) is largely underestimated possibly due to the loss of variability associated with the smoothed output of the decoder $\mu_{NN_\theta}(z, c)$ (section 2.4). We note that, although the VAE parameterizes its latent space as Gaussian, this does not preclude the model from capturing non-Gaussian behavior in its outputs. While the above results clearly prove this point, we emphasize that the Gaussian formulation of the latent space does not translate to the output since the decoder transformation is non-linear. All of the above suggests that there is a trade-off in using the decoder noise under the simple formulation of Eq. 6. This becomes more important for variables such as precipitation with stronger non-Gaussian behavior where more expressive models, or better formulation of decoder noise might be required. Given that all other relevant metrics examined here are largely improved and in close agreement with the population in the VAE+DN model (section 2.5), especially with respect to underdispersivity, and given the importance of representing and quantifying extremes, we encourage the use of decoder noise despite its simplicity and its impact on the skewness of the distribution.

Further evaluation of extremes reinforce this point. The composite of the 99-percentile TAS anomaly maps, computed separately for the population and boosted ensemble (Figure 3c,d), show close agreement between the two (0.97 pattern correlation and $0.85 \text{ } ^\circ\text{C}$ RMSE). VAE+DN reproduces the large TAS anomalies of the higher latitudes, although it has warm biases in a few regions including the Labrador Sea and Southern Ocean (Fig. S4). Comparing with the skewness maps (Fig. 3), these are regions where the negative asymmetry in the population is underestimated in the VAE+DN (similar to the behav-

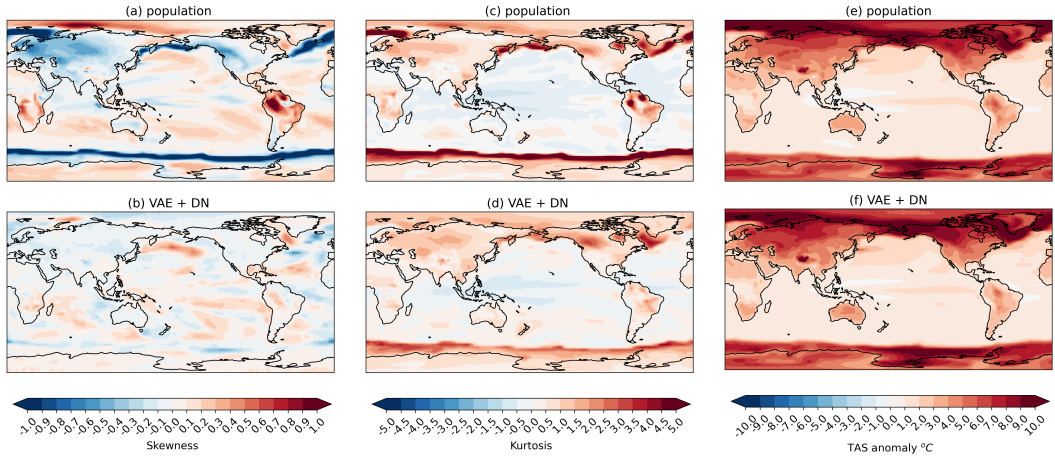


Figure 3: a, b) Maps of skewness (c), (d) kurtosis and (e), (f) %0.99 percentile of TAS anomalies for population (top row) and VAE+DN (bottom row)

ior for Vancouver in Fig. 2d) giving rise to the overestimation of the 99-percentile. Regardless, there is clear and meaningful agreement in both global patterns and magnitude.

In summary, these comparisons show that the simple VAE+DN model is able to generate events outside the training sample, even in regions where non-Gaussian behavior exists. This indicates that the model learns the underlying distribution of the data and generates realizations that are representative of the population. As the skewness maps show, the largest discrepancies are in capturing asymmetries in distributions, leading to overestimation of extremes in some locations. While these results are satisfactory, we anticipate that a more robust treatment of decoder noise, whether through an improved noise formulation or more expressive VAE architectures leading to less structured residuals (i.e., a more accurate decoder mean), will further enhance performance. In this section, we evaluated regional statistics. Next, we evaluate whether the model captures global dependencies and physically-meaningful patterns and teleconnections resulting from dominant modes of climate variability.

3.2 Global structure and teleconnections

VAE models (more generally models with MSE loss function) are trained to maximize the log likelihood of the marginal (here conditional) distributions, i.e, reference value at each grid cell. An important test to assess whether the generated fields do not result from hallucination or overfitting to the marginals is to check if they represent physically meaningful patterns and cross-location dependencies. El Niño Southern Ocean oscillation (ENSO) is the dominant mode of climate variability on seasonal to interannual time scales, driving regional weather and climate conditions, including extremes, through well-known teleconnections. A widely used indicator of ENSO is the Niño3.4 index, which we compute as the monthly TAS anomalies averaged over the Niño 3.4 region (5S-5N, 170W-120W). We start by assessing the statistical properties of the generated Niño 3.4 index.

QQ plots of the Niño3.4 index (Fig. 4a) show excellent agreement for the VAE+DN and population percentiles, despite the poor performance in the lower and upper percentiles of the training data. Moreover, Fig. 4b confirms that while the training data fail to represent extreme ENSO events, as indicated by the tails of the PDFs, the boosted ensemble correctly encompasses the variability and extremes in the population. This is

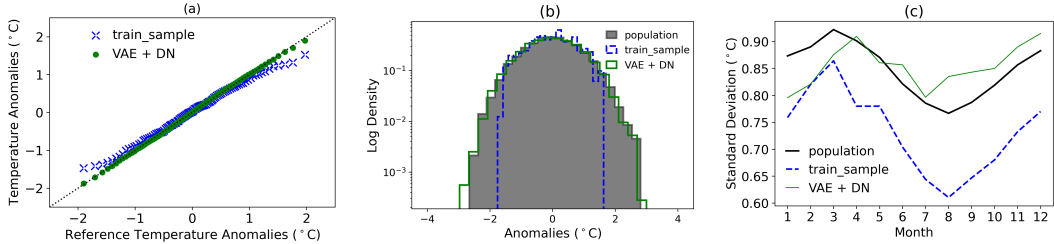


Figure 4: a) QQ plots (b) PDF and (c) seasonal cycle of variability in Niño3.4 index for different data products

also apparent in Figure 4c showing the seasonal cycle for the standard deviation of the Niño3.4 index. Despite the underestimated variability in the training sample, the boosted ensembles largely reproduces the seasonal cycle of the population, although there are slight disagreements, notably in the timing of maximum and minimum variance. This behavior is not surprising, since VAE+DN does not model the time dependence explicitly but infers it from the condition, and the input is standardized using seasonal statistics calculated from limited training data. It is consistent, for instance, with the seasonal cycle for TAS anomalies in the four locations discussed in section 3.1 (Fig. S5 of the supplements). We expect approaches that take into account time dependence, such as VAE + LSTM as in (Sorensen et al., 2024), to improve the time dependence.

Having demonstrated that the VAE+DN model produces TAS fields with a meaningful Niño3.4 index beyond the training sample, we evaluate whether known ENSO teleconnection patterns are present in the boosted ensemble. Figure 5 compares the composite maps obtained by averaging the TAS anomalies for three categories of El Niño events, defined as the Niño3.4 index above the percentiles 75th and 85th, and above the highest value in the training data. We compute the percentiles by pooling data from all months, with the latter category representing extreme ENSO events in the boosted ensemble that are absent from the training data. Prior to this computation, we linearly detrend the ensemble members at each month to emphasize interannual variations relevant to ENSO. The rationale is that strong El Niño events drive TAS anomalies in teleconnected regions that on average follow known warming and cooling patterns. For example, strong El Niño episodes, which are characterized by high temperatures in the tropical Pacific, tend to warm western Canada and Alaska, Southeast Asia, Southeast Africa, parts of Australia, and tropical regions of South America, and cool the southern United States and eastern portions of the extratropics in South America. If such patterns are well represented in the CanESM5 raw ensemble, then a physically meaningful generated ensemble trained on CanESM5 data must also represent those patterns.

As Fig. 5 shows, the generated TAS patterns agree very well with those of the population, particularly in the regions of known teleconnections listed above. There is no expectation of agreement outside those regions, as the variability there is not necessarily linked to ENSO. The cold anomalies over southern United States appear to be slightly reduced in the boosted ensemble, especially for the absent-from-training category, possibly due to underrepresentation of very extreme El Niño events for the linearly detrended index (Fig. S7). Same conclusions hold for La Niña events (Fig. S8) with closely matching patterns of teleconnections but stronger magnitudes of anomalies consistent with overestimation of extreme La Niña events in the linearly detrended index (Fig. S7). The disagreements are mainly the result of biases associated with the small training sample, and the condition embedding coming from a single training realization. In the case of climate projections, we expect improvements for a conditioning that better isolates external forcing, for example, as obtained from the ensemble average of two or more members. The

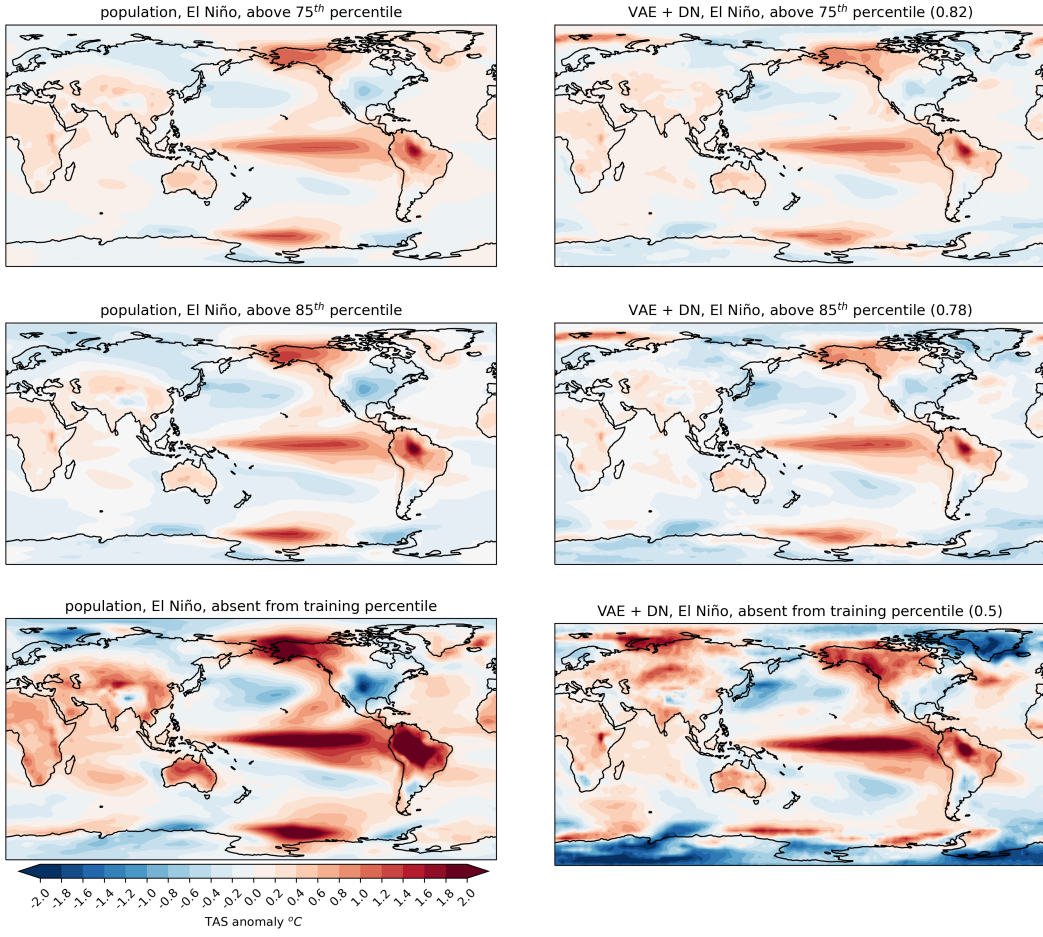


Figure 5: Composites of the linearly detrended monthly TAS anomalies for El-Niño events classified using the 75th, 85th and absent from training percentiles based on the Niño3.4 index (rows). First column is the population dataset and the second column is the boosted ensemble from VAE+DN model.

use of a single realization is in line with applications to predictions, since it is desirable to reproduce the phasing of the predictable internal modes of climate variability, such as ENSO.

Finally, to further assess the global structure and physical realism of the generated ensemble, we examine the radially averaged spectral power of the full TAS fields (not anomalies) across all realizations, averaged over DJF and JJA seasons during 1980-2020. Figure S9 shows a close correspondence to the population indicating the that cVAE model is able to reproduce well the variability across spatial scales, the exception being scales below ~ 200 kms for which there is a small positive bias (consistent with Fig. 1 for TAS anomalies). Those spatial scales are on the order of CanESM5 resolution in and near the tropics. Overall, these results demonstrate that the generated samples reproduce physically meaningful events consistent with the underlying climate. Moreover, they show that the cVAE model is not simply memorizing the input data but learns the underlying climate distribution and is able to produce out-of-distribution samples, even when trained on an extremely limited dataset.

4 Summary and conclusions

We employed a conditional Variational Autoencoder, a class of generative machine learning models, to boost the ensemble size of climate simulations given only a single realization of a reference dataset. The work is motivated by the computational limitations of climate models and the resulting trade-off between increasing the ensemble size or the models spatial resolution. Sufficiently large ensembles of climate predictions and projections are critical to inform policy in the face of climate change and the changing frequency of extremes. A large ensemble would help quantifying uncertainty, the likelihood of extreme, the occurrence of low-probability and high-impact events, and to support long-term decision-making. This is one avenue where generative ML can be effective and provide solutions.

Generative models offer powerful means to learn the underlying distribution of high-dimensional climate fields, making them attractive tools for enhancing climate simulation ensembles. However, the strong non-stationarity of climate data, combined with their limited availability, typically at monthly frequency, present challenges to apply generative models without adaptations. A workaround is to use climate emulators trained on simulations produced with physics-based climate models. In this study, we propose an alternative approach in which we expand ensembles of climate simulations in post-processing by training a generative model with as little as one ensemble member. We demonstrated that even with such a small training sample and with relatively simple model architectures, we can generate large ensembles of physically meaningful simulations. We emphasize that our goal is not to develop the most skillful generative model but rather to create an accessible, simple framework for large-ensemble generation of physically relevant climate simulations, laying the foundation for future work with more advanced models and techniques.

We increased the ensemble size of historical and SSP2-4.5 TAS simulations produced with CCCma's Canadian Earth system model CanESM5 contributed to CMIP6. We trained a cVAE with monthly snapshots of TAS fields from a single realization of the CanESM5 ensemble, conditioned on a low-dimensional vector acquired from the same TAS maps. The condition embedding was designed to capture the dominant modes of (predictable) variability in the data, including those arising from external forcing. The trained cVAE was then used at inference time to generate a large TAS field ensemble by sampling the model's latent distribution (Eq. 8). Our approach was validated by comparing the boosted ensemble with the full 24-member CanESM5 ensemble (excluding training data) for the 1980-2020 period. We showed that the cVAE effectively learns the underlying distribution of TAS anomalies across both regional and global spatial scales, and it generalizes well to produce physically meaningful TAS fields. Its ability to reproduce extremes and well-known ENSO teleconnection patterns in the population beyond its training data further supports the reliability of the boosted ensemble. The conclusions of this work do not change if a different, randomly chosen ensemble member is used for training. This is supported by the close agreement between statistics of the generated ensemble and the full CanESM5 ensemble over the time scale of analysis. We discussed where the variability inherited from the training sample through conditioning might affect the results (e.g. for the detrended ENSO index), but the conclusions remain unaffected. While learning the predictable internal variability from conditioning is desirable for (phase-locked) seasonal-to-decadal predictions, this is suboptimal in the case for estimating long-term uncertainty. For climate projections, we expect that better isolating the forced component in the condition and using more realizations for training will improve the model's ability to estimate long-term uncertainty of the forced trend, especially resulting from slow evolving variability.

The broader objective of this study is to apply this methodology to operational predictions and projections, helping to boost ensemble sizes during post-processing. In doing so, the challenge of underdispersivity in generative machine learning merits special

attention to adequately represent forecast uncertainty and extremes. For the approach followed in this study, we point out two sources of underdispersivity in relation to extremes, one being the non-Gaussian structure of the latent space away from the Gaussian prior and another the loss of variability due to improper formulation of decoder noise, for instance, when MSE is used as a reconstruction loss. We discussed approximations to the latent distribution and the covariance noise structure in the decoder, estimated from the training stage, which greatly improve underdispersivity and performance. We showed that understanding the variability in the model output, generated by the decoder, is especially important for accurate representation of the climate system given the presence of complex spatio-temporal variability in the climate data and its unpredictable weather-induced noise component. In fact, we would argue that the issue of spectral loss in ML models could largely be attributed to deep learning models that often implicitly solve a probability density approximation for a Gaussian output distribution. As a result, variability in the output distribution becomes important for the representation of the fine-scale structure, rather than simply training with a loss function that drives the convergence of the output to the mean, in the case of mean square error, or the median, in the case of mean absolute error (Goodfellow et al., 2016).

Future studies will use this framework for climate simulations at higher resolutions, multi-variable ensemble generation, boosting ensembles of CMIP6 scenario runs and seasonal-to-decadal predictions, and for observation-based ensembles to assess limits of predictability and probability of extremes. Moreover, the framework proposed in this study does not explicitly model the time dependence. This can be addressed using autoregressive methods or recurrent neural networks. We recommend either modeling decoder variability as a function of the data whenever possible or providing clear guidelines and explanations when using approximations or more advanced ML techniques. Finally, we expect more expressive and optimally tuned architectures to reduce the biases associated with residual structure in decoder noise.

Open Research Section

The data from the CanESM5 model (Swart et al., 2019b) used in the study are publicly available through Earth System Grid Federation (ESGF) data storage servers such as https://aims2.llnl.gov/search/cmip6/?mip_era=CMIP6&activity_id=CMIP&institution_id=CCCMa&source_id=CanESM5-1&experiment_id=piControl. Python codes for training the cVAE models, generating outputs and manuscript analysis/figures can be accessed through https://github.com/ParsaGooya/CCCMa_boostENS_JGRMLComp. All other inquiries should be directed to P. Gooya. (Publication ready and cleaned-up version of codes are being prepared and will be available before final publication.)

Conflict of interest

The authors declare no conflicts of interest.

Acknowledgments

We thank Dr. Bill Merryfield for his valuable comments on an earlier version of the paper.

References

An, S., & Jeon, J.-J. (2023). Distributional learning of variational autoencoder: Application to synthetic data generation. , 36, 57825–57851. Retrieved from https://proceedings.neurips.cc/paper_files/paper/2023/file/b456a00e145ad56f6f251f79f8c8a7de-Paper-Conference.pdf

Barthel Sorensen, B., Charalampopoulos, A., Zhang, S., Harrop, B. E., Leung, L. R., & Sapsis, T. P. (2024). A non-intrusive machine learning framework for de-biasing long-time coarse resolution climate simulations and quantifying rare events statistics. *Journal of Advances in Modeling Earth Systems*, 16(3), e2023MS004122. Retrieved from <https://agupubs.onlinelibrary.wiley.com/doi/abs/10.1029/2023MS004122> (e2023MS004122 2023MS004122) doi: <https://doi.org/10.1029/2023MS004122>

Boer, G. J., Kharin, V. V., & Merryfield, W. J. (2013). Decadal predictability and forecast skill. *Climate Dynamics*, 41, 1817–1833. Retrieved from <https://link.springer.com/article/10.1007/s00382-013-1705-0> doi: 10.1007/s00382-013-1705-0

Daust, K., & Monahan, A. (2024). Capturing climatic variability: Using deep learning for stochastic downscaling. *arXiv preprint arXiv:2406.02587*. (Submitted to Artificial Intelligence for the Earth Systems AMS Journal) doi: 10.48550/arXiv.2406.02587

Dhariwal, P., & Nichol, A. (2021). Diffusion models beat GANs on image synthesis. , 34, 8780–8794.

Dorta, G., Vicente, S., Agapito, L., Campbell, N. D. F., & Simpson, I. (2018). *Structured uncertainty prediction networks*. Retrieved from <https://arxiv.org/abs/1802.07079>

Eyring, V., Bony, S., Meehl, G. A., Senior, C. A., Stevens, B., Stouffer, R. J., & Taylor, K. E. (2016). Overview of the coupled model intercomparison project phase 6 (cmip6) experimental design and organization. *Geoscientific Model Development*, 9(5), 1937–1958. Retrieved from <https://gmd.copernicus.org/articles/9/1937/2016/> doi: 10.5194/gmd-9-1937-2016

Ghosh, P., Sajjadi, M. S. M., Vergari, A., Black, M., & Schölkopf, B. (2020). *From variational to deterministic autoencoders*. Retrieved from <https://arxiv.org/abs/1903.12436>

Goodfellow, I., Bengio, Y., & Courville, A. (2016). *Deep learning*. MIT Press. (<http://www.deeplearningbook.org>)

Goodfellow, I., Pouget-Abadie, J., Mirza, M., Xu, B., Warde-Farley, D., Ozair, S., ... Bengio, Y. (2014). Generative adversarial nets. , 27. Retrieved from https://proceedings.neurips.cc/paper_files/paper/2014/file/5ca3e9b122f61f8f06494c97b1afccf3-Paper.pdf

Gooya, P., & Sospedra-Alfonso, R. (2025). Probabilistic bias adjustment of seasonal predictions of arctic sea ice concentration. In *Neurips 2025 workshop on tackling climate change with machine learning*. Retrieved from <https://www.climatechange.ai/papers/neurips2025/87>

Gooya, P., Swart, N. C., & Hamme, R. C. (2023). Time-varying changes and uncertainties in the cmip6 ocean carbon sink from global to local scale. *Earth System Dynamics*, 14(2), 383–398. Retrieved from <https://esd.copernicus.org/articles/14/383/2023/> doi: 10.5194/esd-14-383-2023

Grönquist, P., Yao, C., Ben-Nun, T., Dryden, N., Dueben, P., Li, S., & Hoe-fler, T. (2021). Deep learning for post-processing ensemble weather forecasts. *Philosophical Transactions of the Royal Society A: Mathematical, Physical and Engineering Sciences*, 379(2194), 20200092. Retrieved from <https://royalsocietypublishing.org/doi/abs/10.1098/rsta.2020.0092> doi: 10.1098/rsta.2020.0092

Ho, J., Chan, W., Saharia, C., Whang, J., Gao, R., Gritsenko, A., ... Salimans, T. (2022, October). *Imagen video: High definition video generation with diffusion models*. arXiv preprint *arXiv:2210.02303*. (arXiv:2210.02303 [cs.CV], 5 October 2022)

Hsieh, M.-K., & Wu, C.-M. (2024). Developing an explainable variational autoencoder (vae) framework for accurate representation of local circulation in taiwan. *Journal of Geophysical Research: Atmospheres*, 129(12), e2024JD041167.

Retrieved from <https://agupubs.onlinelibrary.wiley.com/doi/abs/10.1029/2024JD041167> (e2024JD041167 2024JD041167) doi: <https://doi.org/10.1029/2024JD041167>

Kingma, D. P., & Welling, M. (2022). *Auto-encoding variational bayes*. Retrieved from <https://arxiv.org/abs/1312.6114>

Lai, C.-Y., Hassanzadeh, P., Sheshadri, A., Sonnewald, M., Ferrari, R., & Balaji, V. (2025). Machine learning for climate physics and simulations [Journal Article]. *Annual Review of Condensed Matter Physics*, 16(Volume 16, 2025), 343-365. Retrieved from <https://www.annualreviews.org/content/journals/10.1146/annurev-conmatphys-043024-114758> doi: <https://doi.org/10.1146/annurev-conmatphys-043024-114758>

Lehner, F., Deser, C., Maher, N., Marotzke, J., Fischer, E. M., Brunner, L., ... Hawkins, E. (2020). Partitioning climate projection uncertainty with multiple large ensembles and cmip5/6. *Earth System Dynamics*, 11(2), 491–508. Retrieved from <https://esd.copernicus.org/articles/11/491/2020/> doi: [10.5194/esd-11-491-2020](https://doi.org/10.5194/esd-11-491-2020)

Leutbecher, M. (2019). Ensemble size: How suboptimal is less than infinity? *Quarterly Journal of the Royal Meteorological Society*, 145(S1), 107-128. Retrieved from <https://rmets.onlinelibrary.wiley.com/doi/abs/10.1002/qj.3387> doi: [10.1002/qj.3387](https://doi.org/10.1002/qj.3387)

Li, L., Carver, R., Lopez-Gomez, I., Sha, F., & Anderson, J. (2024). Generative emulation of weather forecast ensembles with diffusion models. *Science Advances*, 10(13), eadk4489. Retrieved from <https://www.science.org/doi/abs/10.1126/sciadv.adk4489> doi: [10.1126/sciadv.adk4489](https://doi.org/10.1126/sciadv.adk4489)

Lopez-Gomez, I., Wan, Z. Y., Zepeda-Núñez, L., Schneider, T., Anderson, J., & Sha, F. (2024). Dynamical-generative downscaling of climate model ensembles. *arXiv preprint arXiv:2410.01776v1*. doi: [10.48550/arXiv.2410.01776](https://doi.org/10.48550/arXiv.2410.01776)

Lupin-Jimenez, L., Darman, M., Hazarika, S., Wu, T., Gray, M., He, R., ... Chat-topadhyay, A. (2025). Simultaneous emulation and downscaling with physically-consistent deep learning-based regional ocean emulators. *arXiv preprint arXiv:2501.05058*. doi: [10.48550/arXiv.2501.05058](https://doi.org/10.48550/arXiv.2501.05058)

Merryfield, W. J., Baehr, J., Batté, L., Becker, E. J., Butler, A. H., Coelho, C. A. S., ... Yeager, S. (2020). Current and emerging developments in subseasonal to decadal prediction. *Bulletin of the American Meteorological Society*, 101(6), E869–E896. Retrieved from <https://doi.org/10.1175/BAMS-D-19-0037.1> doi: [10.1175/BAMS-D-19-0037.1](https://doi.org/10.1175/BAMS-D-19-0037.1)

Mooers, G., Tuyls, J., Mandt, S., Pritchard, M., & Beucler, T. G. (2021). Generative modeling of atmospheric convection. , 98–105. Retrieved from <https://doi.org/10.1145/3429309.3429324> doi: [10.1145/3429309.3429324](https://doi.org/10.1145/3429309.3429324)

Nerini, D., Besic, N., Sideris, I., Germann, U., & Foresti, L. (2017). A non-stationary stochastic ensemble generator for radar rainfall fields based on the short-space fourier transform. *Hydrol. Earth Syst. Sci.*, 21, 2777–2797. Retrieved from <https://doi.org/10.5194/hess-21-2777-2017> doi: [10.5194/hess-21-2777-2017](https://doi.org/10.5194/hess-21-2777-2017)

Oliveira, D. A. B., Diaz, J. G., Zadrozny, B., Watson, C. D., & Zhu, X. X. (2022). Controlling weather field synthesis using variational autoencoders. , 5027-5030. doi: [10.1109/IGARSS46834.2022.9884668](https://doi.org/10.1109/IGARSS46834.2022.9884668)

Price, I., Sanchez-Gonzalez, A., Alet, F., Andersson, T. R., El-Kadi, A., Masters, D., ... Willson, M. (2025). Probabilistic weather forecasting with machine learning. *Nature*, 637(8044), 84–90. Retrieved from <https://doi.org/10.1038/s41586-024-08252-9> doi: [10.1038/s41586-024-08252-9](https://doi.org/10.1038/s41586-024-08252-9)

Prince, S. J. (2023). *Understanding deep learning*. The MIT Press. Retrieved from <http://udlbook.com>

Rezende, D. J., Mohamed, S., & Wierstra, D. (2014, 22–24 Jun). Stochastic backpropagation and approximate inference in deep generative models. ,

32(2), 1278–1286. Retrieved from <https://proceedings.mlr.press/v32/rezende14.html>

Rombach, R., Blattmann, A., Lorenz, D., Esser, P., & Ommer, B. (2022). High-resolution image synthesis with latent diffusion models. , 10684–10695. Retrieved from <https://github.com/CompVis/latent-diffusion>

Rühling Cachay, S., Henn, B., Watt-Meyer, O., Bretherton, C. S., & Yu, R. (2024). Probabilistic emulation of a global climate model with spherical diffusion. *arXiv preprint arXiv:2406.14798v2*. (NeurIPS 2024 submission; code is available at the provided URL.) doi: 10.48550/arXiv.2406.14798

Sacco, M., Ruiz, J., Pulido, M., & Tandeo, P. (2022, August). Evaluation of Machine Learning Techniques for Forecast Uncertainty Quantification. *Quarterly Journal of the Royal Meteorological Society*, 148(749), 3470-3490. Retrieved from <https://imt-atlantique.hal.science/hal-03685523> doi: 10.1002/qj.4362

Sankarapandian, S., & Kulis, B. (2021). β -annealed variational autoencoder for glitches. Retrieved from <https://arxiv.org/abs/2107.10667>

Sohn, K., Lee, H., & Yan, X. (2015). Learning structured output representation using deep conditional generative models. , 28. Retrieved from https://proceedings.neurips.cc/paper_files/paper/2015/file/8d55a249e6baa5c06772297520da2051-Paper.pdf

Sorensen, B. B., Zepeda-Núñez, L., Lopez-Gomez, I., Wan, Z. Y., Carver, R., Sha, F., & Sapsis, T. (2024). A probabilistic framework for learning non-intrusive corrections to long-time climate simulations from short-time training data. Retrieved from <https://arxiv.org/abs/2408.02688>

Sospedra-Alfonso, R., & Boer, G. J. (2020). Assessing the impact of initialization on decadal prediction skill. *Geophysical Research Letters*, 47(4), e2019GL086361. Retrieved from <https://doi.org/10.1029/2019GL086361> doi: 10.1029/2019GL086361

Sospedra-Alfonso, R., Merryfield, W. J., Boer, G. J., Kharin, V. V., Lee, W.-S., Seiler, C., & Christian, J. R. (2021). Decadal climate predictions with the canadian earth system model version 5 (canesm5). *Geoscientific Model Development*, 14(11), 6863–6891. Retrieved from <https://gmd.copernicus.org/articles/14/6863/2021/> doi: 10.5194/gmd-14-6863-2021

Subich, C., Husain, S. Z., Separovic, L., & Yang, J. (2025). Fixing the double penalty in data-driven weather forecasting through a modified spherical harmonic loss function. Retrieved from <https://arxiv.org/abs/2501.19374>

Swart, N. C., Cole, J. N., Kharin, V. V., Lazare, M., Scinocca, J. F., Gillett, N. P., ... Reader, C. (2019b). Cccma canesm5.1 model output prepared for cmip6 cmip piconcontrol. Earth System Grid Federation. Retrieved from <https://doi.org/10.22033/ESGF/CMIP6.17424> doi: 10.22033/ESGF/CMIP6.17424

Swart, N. C., Cole, J. N. S., Kharin, V. V., Lazare, M., Scinocca, J. F., Gillett, N. P., ... Winter, B. (2019a). The canadian earth system model version 5 (canesm5.0.3). *Geoscientific Model Development*, 12(11), 4823–4873. Retrieved from <https://gmd.copernicus.org/articles/12/4823/2019/> doi: 10.5194/gmd-12-4823-2019

Szwarcman, D., Guevara, J., Macedo, M. M. G., Zadrozny, B., Watson, C., Rosa, L., & Oliveira, D. A. B. (2024, Feb 9). Quantizing reconstruction losses for improving weather data synthesis. *Scientific Reports*, 14(1), 3396. Retrieved from <https://doi.org/10.1038/s41598-024-52773-2> doi: 10.1038/s41598-024-52773-2

Wang, M., Sorensen, B. B., & Sapsis, T. (2025). Gen2: A generative prediction-correction framework for long-time emulations of spatially-resolved climate extremes. Retrieved from <https://arxiv.org/abs/2508.15196>